

# Spectroscopic Investigations under *in vivo* Conditions Reveal the Complex Metal Hydride Chemistry of [FeFe]-hydrogenase

Lívía S. Mészáros<sup>[a], ‡</sup>, Pierre Ceccaldi<sup>[a], ‡</sup>, Marco Lorenzi<sup>[a]</sup>, Holly J. Redman<sup>[a]</sup>, Emanuel Pfitzner<sup>[b]</sup>, Joachim Heberle<sup>[b]</sup>, Moritz Senger<sup>[b]</sup>, Sven T. Stripp<sup>[b]\*</sup> and Gustav Berggren<sup>[a]\*</sup>

[a] L. S. Mészáros, P. Ceccaldi, M. Lorenzi, H. J. Redman, G. Berggren; Molecular Biomimetics, Dept. of Chemistry – Ångström Laboratory; Uppsala University; Lägerhyddsvägen 1, SE-75120, Uppsala, Sweden

[b] E. Pfitzner, J. Heberle, M. Senger, S. T. Stripp; Institute of Experimental Physics, Experimental Molecular Biophysics; Freie Universität Berlin; Arnimallee 14, DE-14195, Berlin, Germany

**ABSTRACT:** Hydrogenases are among the fastest H<sub>2</sub> evolving catalysts known to date and have been extensively studied under *in vitro* conditions. Here, we report the first mechanistic investigation of an [FeFe]-hydrogenase under *in vivo* conditions. Functional [FeFe]-hydrogenase from the green alga *Chlamydomonas reinhardtii* is generated in genetically modified *Escherichia coli* cells, by addition of a synthetic cofactor to the growth medium. The assembly and reactivity of the resulting semi-synthetic enzyme was monitored using whole-cell electron paramagnetic resonance as well as Fourier-transform infrared spectroscopy. Through a combination of gas treatments, pH titrations and isotope editing, we were able to corroborate the physiological relevance of a number of proposed catalytic intermediates, including reactive iron-hydride species. We demonstrate the formation of the so-called hydride state *in vivo*. Moreover, two previously uncharacterized redox species are reported herein, illustrating the complex metal hydride chemistry of [FeFe]-hydrogenase.

## INTRODUCTION

Hydrogenases are gas processing metalloenzymes that interconvert protons and molecular hydrogen ( $H_2$ ) with remarkable efficiency. The so-called [FeFe]-hydrogenases are considered the most efficient  $H_2$  producers in nature, with reported turnover frequencies up to  $10,000 H_2 s^{-1}$ .<sup>1-2</sup> This remarkable activity makes [FeFe]-hydrogenases highly relevant for biotechnological  $H_2$  production as an alternative to platinum-based electrolysis<sup>3-6</sup> and a biological blue-print for the design of synthetic catalysts.<sup>7-9</sup> Consequently, intense efforts have been invested in elucidating the structure and catalytic mechanism of these enzymes.<sup>10-11</sup>

The reactivity of [FeFe]-hydrogenases is enabled by a hexanuclear iron complex, referred to as the “H-cluster” (Fig. 1A). This cofactor consists of a canonical iron-sulfur cluster ( $[4Fe-4S]_H$ ) coupled to an organometallic diiron subsite ( $[2Fe]_H$ ). The low-valent iron ions of the  $[2Fe]_H$  subsite are bridged by an azadithiolate group ( $^-SCH_2NHCH_2S^-$ , adt) and further coordinated by carbon monoxide (CO) and cyanide ( $CN^-$ ) ligands.<sup>12-15</sup> Due to its unique nature, the biosynthesis of the  $[2Fe]_H$  subsite requires at least three hydrogenase specific maturation enzymes.<sup>16-20</sup> Despite challenges in preparing the enzyme, extensive *in vitro* work has revealed a number of potential catalytic intermediates. The oxidized resting state of the enzyme ( $H_{ox}$ ) exhibits a mixed-valence  $[2Fe]_H$  subsite and an oxidized  $[4Fe-4S]_H$  cluster ( $[4Fe-4S]_H^{2+}-[Fe(I)Fe(II)]_H$ ).<sup>21-22</sup> Under acidic conditions  $H_{ox}H$  is formed, attributed to a protonation at the  $[4Fe-4S]_H$  cluster.<sup>23-24</sup> Reduction of  $H_{ox}$  by one electron results in either  $H_{red}'$  or  $H_{red}$  (the latter also referred to as “ $H_{red}H^+$ ”).<sup>23, 25-26</sup> The H-cluster shows a reduced and possibly protonated  $[4Fe-4S]_H$  cluster in  $H_{red}'$  whereas in  $H_{red}$  the  $[2Fe]_H$  site is reduced and protonated.<sup>27</sup> Further reduction of  $H_{red}$  generates the “super-reduced” state,  $H_{sred}$ , identified as a  $[4Fe-4S]_H^+-[Fe(I)Fe(I)]_H$  species.<sup>28</sup>

The exact nature of these intermediate states and their relevance to the catalytic mechanism is under debate.<sup>10, 27, 29</sup> However, all recent models agree that a terminal hydride is stabilized during catalysis. Heterolytic cleavage of H<sub>2</sub> is proposed to result in the so-called hydride state, H<sub>hyd</sub>, featuring a terminal hydride on the [2Fe]<sub>H</sub> subsite (Fig. 1A). The electronic structure of this state has been shown to comprise a diamagnetic [Fe(II)Fe(II)]<sub>H</sub> subsite coupled to a paramagnetic [4Fe-4S]<sub>H</sub><sup>+</sup> cluster. This intermediate has recently been detected *in vitro* and shown to accumulate in amino acid variants with disrupted proton transfer networks, but also in native enzyme under reducing low pH conditions.<sup>30-32</sup>

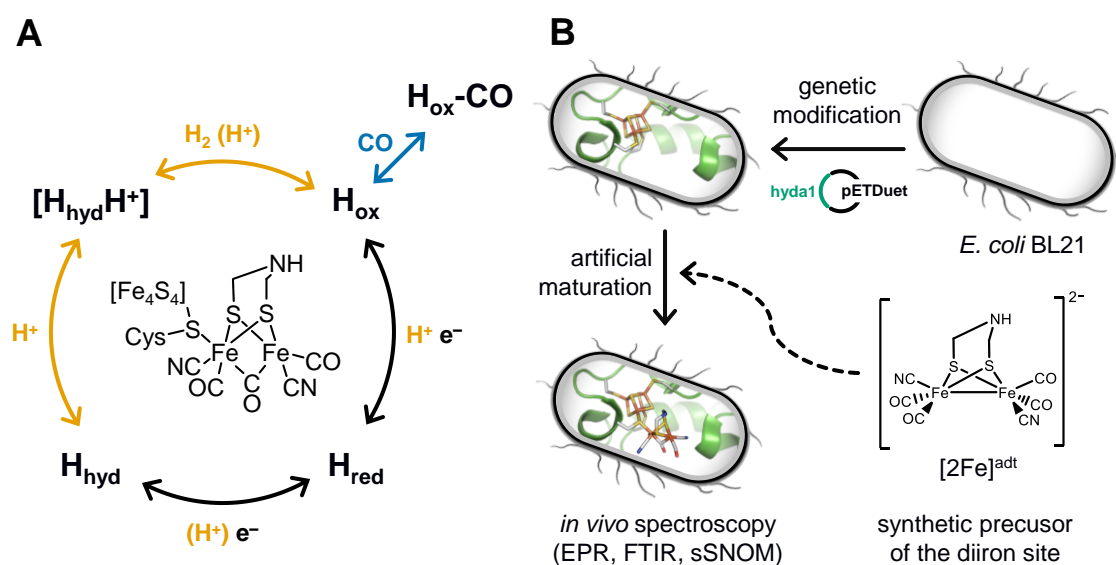


**Figure 1.** Catalytic mechanism and H-cluster assembly. **(A)** Schematic representation of the oxidized H-cluster and the catalytic cycle of [FeFe]-hydrogenase. Here, proposed key intermediates were observed *in vivo* for the first time, and conditions for accumulating a protonated hydride state (denoted H<sub>hyd</sub>H<sup>+</sup>) are reported. Referred to as H<sub>red</sub>, different one-electron reduced H-cluster species are conceivable. The catalytic cycle is derived from refs. 10 and 32, debated protonation steps shown in parenthesis. **(B)** Genetic modification of *E. coli* for expression of [FeFe] hydrogenase apoprotein, followed by synthetic maturation generates functional hydrogenase (the H-cluster is shown in the H<sub>ox</sub> state). The reactivity of this semi-synthetic enzyme is probed in whole cells by EPR and ATR FTIR spectroscopy. In parallel, the integrity of the cells is verified by AFM and near-field IR spectroscopy and imaging.

The biological maturation machinery required for H-cluster assembly can be circumvented by incubating [FeFe]-hydrogenase apo-protein with synthetic mimics of the [2Fe]<sub>H</sub> subsite. It is well established that, under *in vitro* conditions, the incorporation of the [Fe<sub>2</sub>(adt)(CO)<sub>4</sub>(CN)<sub>2</sub>]<sup>2-</sup> complex ([2Fe]<sup>adt</sup>) results in the spontaneous assembly of semi-synthetic hydrogenases indistinguishable from the native enzyme ([2Fe]<sup>adt</sup>-HydA1).<sup>7, 13, 33-35</sup> We recently adapted this strategy for *in vivo* applications, enabling the preparation of fully functional semi-synthetic enzymes in both *E. coli* and cyanobacteria.<sup>6, 36-37</sup> Herein, we take advantage of this protocol to perform spectroscopic investigations of [FeFe]-hydrogenase under *in vivo* conditions (Fig. 1B). We combine whole-cell electron paramagnetic resonance (EPR) and Fourier-transform infrared (FTIR) spectroscopy in order to characterize the enzymatic activity and catalytic mechanism of an [FeFe]-hydrogenase from the photosynthetic green algae *Chlamydomonas reinhardtii*, HydA1.<sup>38</sup> In parallel, single cells were characterized by atomic force microscopy (AFM), scattering scanning near-field optical microscopy (sSNOM) and nano-FTIR spectroscopy, verifying cellular integrity and protein content. The study provides the first demonstration of the formation of reactive metal hydride species in living cells, as the H<sub>hyd</sub> state accumulates *in vivo* under mildly acidic conditions. Through a combination of gas flushes and pH changes we also detected a number of additional proposed catalytic intermediates, including H<sub>ox</sub>, H<sub>ox</sub>H, and H<sub>red</sub>. Moreover, two new hydride-like species are enriched, including one so far undetected species generated at conditions mimicking the native environment of the enzyme, *i.e.* the stroma of the chloroplast in *C. reinhardtii*.

## RESULTS AND DISCUSSION

**In vivo assembly of the semi-synthetic H-cluster.** To generate hydrogenase enzyme in concentrations suitable for whole-cell spectroscopy, HydA1 was heterologously expressed in BL21(DE3) *E. coli* cells, similar to previous reports.<sup>36-37</sup> The absence of the [FeFe]-hydrogenase specific maturation machinery in *E. coli* results in the synthesis of an inactive form of the enzyme containing the [4Fe-4S]<sub>H</sub> cluster but lacking the [2Fe]<sub>H</sub> subsite (apo-HydA1). 50 mL cell cultures were concentrated to 2 mL and depleted of O<sub>2</sub> at which point the synthetic cofactor mimic [2Fe]<sup>adt</sup> was added to the medium, and the H-cluster assembly monitored by EPR spectroscopy and H<sub>2</sub> production assays (for details see Experimental Section). The apo-enzyme remains undetected in our experiments, due to the intensity of underlying signals attributed to other iron-sulfur proteins in *E. coli* (Fig. S1). Conversely, the formation of the H-cluster was readily observable by whole-cell EPR spectroscopy (Fig. 2A). Incubation of the cell suspensions for 1 h in the presence of low concentrations (0.008 – 0.8 μM) of the synthetic [2Fe]<sup>adt</sup> cofactor resulted in the appearance of a rhombic EPR signal attributable to H<sub>ox</sub> (g = 2.100; 2.040; 1.998). For higher concentrations of [2Fe]<sup>adt</sup> in the cell medium (8 – 80 mM), the overall intensity of the EPR signal increased. Quantification of the signals versus a copper standard showed that a final total spin concentration of up to 10 mM was obtained following this protocol (Fig. 2B). However, the spectra became dominated by an axial signal originating from H<sub>ox</sub>-CO (g = 2.054; 2.007).

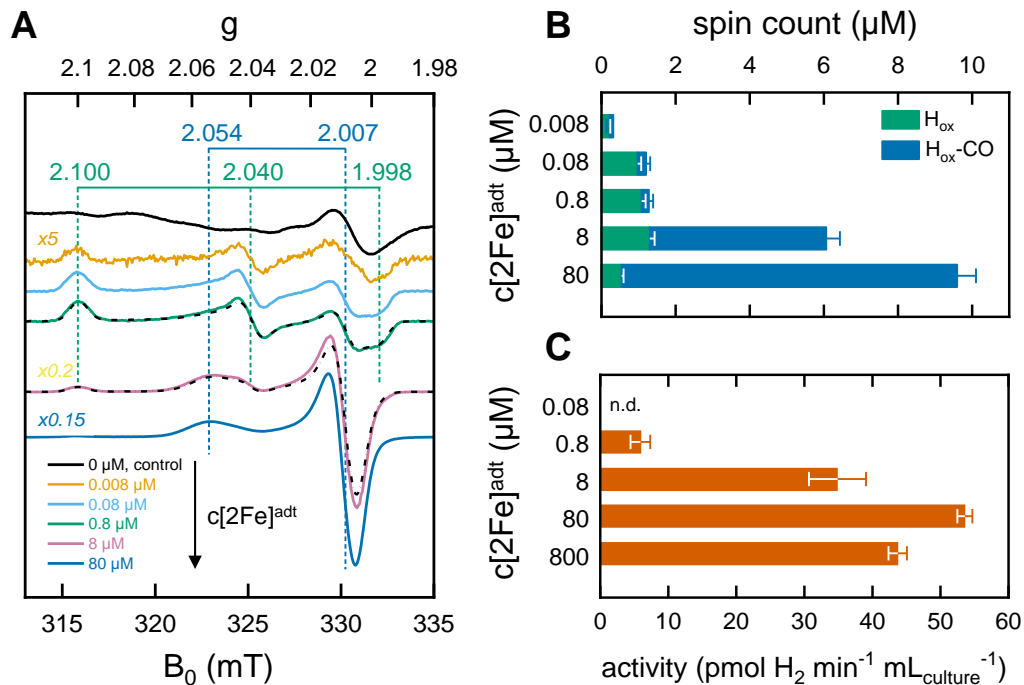


**Figure 2.** *In vivo* H-cluster assembly monitored by EPR spectroscopy and  $H_2$  gas production. **(A)** Whole-cell EPR spectra of apo-HydA1 (control, 0 mM  $[2Fe]^{adt}$  added) and  $[2Fe]^{adt}$ -HydA1 containing cells. H-cluster assembly occurs spontaneously upon addition of  $[2Fe]^{adt}$  to the medium, with  $H_{ox}$  being the favored state at low  $[2Fe]^{adt}$  concentrations. As the concentration of the synthetic cofactor increases, the cell samples become dominated by the  $H_{ox-CO}$  state. The g-values of  $H_{ox}$  (cyan dashed lines) and  $H_{ox-CO}$  (blue dashed lines) states are based on simulations of the two samples at 0.8 and 8  $\mu M$  (black dash-dotted lines). All  $[2Fe]^{adt}$ -HydA1 spectra were corrected for contribution from the cells by subtracting the signal of the apo-HydA1 control sample. EPR experimental conditions:  $T = 20$  K,  $P = 1$  mW,  $\nu = 9.28$  GHz. **(B)** Concentrations of the  $H_{ox}$  (cyan bars) and  $H_{ox-CO}$  (blue bars) signals in each sample, extrapolated from the simulations. **(C)** Average rate of hydrogen gas production during 1 h from anaerobic 2 mL *E. coli* cultures as a function of  $[2Fe]^{adt}$  concentration in the cell medium; n.d.: not detected.

The successful assembly of functional enzyme was further verified by monitoring  $H_2$  production from the *E. coli* cells suspended in fresh minimal medium.  $H_2$  gas formation was clearly observable after the addition of 0.8  $\mu M$   $[2Fe]^{adt}$  to the medium and increased up to 80  $\mu M$   $[2Fe]^{adt}$ , concomitantly with the overall EPR signal intensity (Fig. 2C). The same trend was also observed

in *in vitro* assays. Hydrogenase activity assays performed on lysed cells demonstrated that a significant fraction (approx. 80%) of the total available apo-HydA1 pool had formed the active  $[2\text{Fe}]^{\text{adt}}$ -HydA1 enzyme after 1h incubation with 80  $\mu\text{M}$   $[2\text{Fe}]^{\text{adt}}$  in the cell medium (Fig. S2). Increasing the concentration of  $[2\text{Fe}]^{\text{adt}}$  beyond this point resulted in a decline of *in vivo*  $\text{H}_2$  production. In light of the dominance of  $\text{H}_{\text{ox}}\text{-CO}$  at higher  $[2\text{Fe}]^{\text{adt}}$  concentration (Fig. 2B), the decreased  $\text{H}_2$  productivity is attributed to release of CO from excess cofactor in the cell medium resulting in inhibition of the enzyme. Consequently, a concentration of 80  $\mu\text{M}$   $[2\text{Fe}]^{\text{adt}}$  in the cell medium was determined as optimal for the following mechanistic studies.

**Monitoring the H-cluster in  $\text{H}_2$  gas producing cell suspensions.** The redox status of the enzyme and stability of the H-cluster in *E. coli* cells was probed by exposing  $\text{H}_2$  producing cells to gases expected to be inert (Ar), reducing ( $\text{H}_2$ ), or potentially inhibiting (CO,  $\text{O}_2$ ). More specifically, the headspace atmosphere of 2 mL cell suspensions were purged with Ar, CO,  $\text{H}_2$ , or incubated on air ( $\text{O}_2$ ) for 1 h and the status of the enzyme analyzed by EPR spectroscopy (Fig. 3 and Fig. S3). At the end of the incubation, the cells were harvested under an Ar atmosphere, thus only lasting changes on the equilibria of H-cluster states were detected. Compared to untreated cell suspension (Fig. 2A, 80 mM spectrum), samples purged with Ar displayed a decrease of  $\text{H}_{\text{ox}}\text{-CO}$  with a concomitant increase of  $\text{H}_{\text{ox}}$  in combination with an overall loss in signal intensity (Fig. 3, Ar spectrum). Cells exposed to CO retained the intense  $\text{H}_{\text{ox}}\text{-CO}$  signal (Fig. 3, CO spectrum), while identical cell suspensions exposed to an  $\text{H}_2$  atmosphere showed similar, but more pronounced behavior to the samples incubated under Ar. The  $\text{H}_{\text{ox}}\text{-CO}$  population was converted into  $\text{H}_{\text{ox}}$  and a slightly larger loss of signal intensity was observed (Fig. 3,  $\text{H}_2$  spectrum). These transitions were fully reversible, as the H-cluster converted back to the  $\text{H}_{\text{ox}}\text{-CO}$  state when  $\text{H}_2$  purged samples were subsequently purged with CO for 1 h.

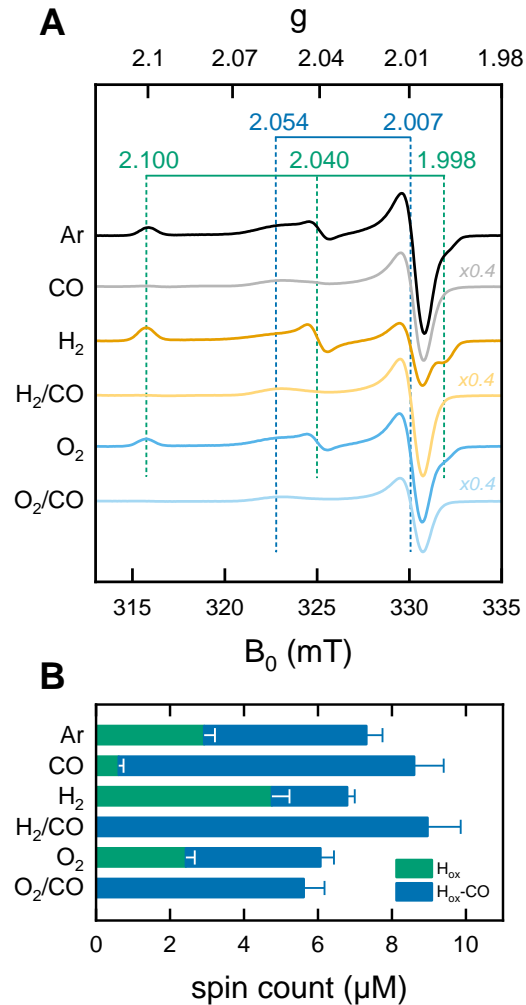


**Figure 3.** Effect of atmosphere on the *in vivo* EPR signatures of the H-cluster. **(a)** Representative EPR spectra observed of whole-cell samples following 1 h incubation under a 100% Ar, CO, H<sub>2</sub> or air (O<sub>2</sub>) atmosphere, revealing transitions between H<sub>ox</sub>-CO, H<sub>ox</sub> and an EPR silent species. Gas treatments were performed on separate samples originating from a common *E. coli* stock culture, in specific cases samples undergo sequential gas treatments as indicated (H<sub>2</sub>/CO and O<sub>2</sub>/CO). Spectra shown after subtraction of an apo-HydA1 control spectrum, similar to Figure 2 black spectrum; EPR experimental conditions: T = 20 K, P = 1 mW,  $\nu$  = 9.28 GHz. **(b)** Spin count of hydrogenase-specific paramagnetic species in each sample, with respective proportions of H<sub>ox</sub> and H<sub>ox</sub>-CO signals based on simulations of the Ar, CO, H<sub>2</sub> and O<sub>2</sub> spectra (Figure S4).

The stability of the H-cluster *in vivo* under aerobic conditions was probed by exposing the cell suspension to air. As observed for Ar and H<sub>2</sub>, this resulted in a decrease of the overall EPR signal intensity, and a conversion from H<sub>ox</sub>-CO to H<sub>ox</sub> (Fig. 3, O<sub>2</sub> spectrum). A subsequent CO flush led to conversion back to the H<sub>ox</sub>-CO state, albeit with a 30 % decrease in signal intensity as compared to the anaerobic samples (Fig. 3B, compare CO, H<sub>2</sub>/CO, and O<sub>2</sub>/CO). This partial instability of the H-cluster upon air exposure was further confirmed by *in vitro* enzymatic assays, in which lysed samples from air-exposed cells showed ca. 70 % activity of strictly anaerobic samples (Fig. S5).

In summary, the CO-inhibited state was slowly lost in the absence of CO (Ar atmosphere) and the enzyme enters the catalytic cycle forming H<sub>ox</sub> and an EPR-silent species. When Ar was exchanged for a reducing H<sub>2</sub> atmosphere a shift from H<sub>ox</sub> in favor of the EPR-silent species was observed, presumably H<sub>red</sub> or H<sub>red</sub>'. The near-quantitative conversion to H<sub>ox</sub>-CO under a CO atmosphere shows that the entire enzyme population is exposed to the headspace atmosphere, despite the dense cell suspensions. Nevertheless, we observed rather limited differences between Ar and H<sub>2</sub> treated cells. On the time-scale of these experiments, the H-cluster apparently re-equilibrates with the redox environment of the cell favoring oxidized species. The influence of the cellular environment was more striking under air, where the O<sub>2</sub> scavenging capacity of *E. coli* ensured that a majority of the enzyme remained intact even after 1 h in the presence of air.

**Investigating the integrity and enzymatic activity of single cells.** The integrity of the cells following formation of [2Fe]<sup>adt</sup>-HydA1 was verified by atomic force microscopy (AFM) on diluted samples (factor 5 x 10<sup>-5</sup>). The topography of the cells suggested viable bacteria (Fig. 4a) and only a limited number of cells were found to be disintegrated (Fig. S6). Subsequently, the local IR absorption of single cells was recorded using scattering-type scanning near-field optical microscopy (sSNOM). This label-free technique provides a chemical image of the cell at a spatial

resolution of 30 nm.<sup>39</sup> The amide I band ( $1665\text{ cm}^{-1}$ ) was used to visualize the protein content in a number of representative cells (Fig. 4B and Fig. S7). The protein distribution was homogenous within the cells and no indication of secreted protein outside the cell was detected. Moreover, nano-FTIR near-field phase spectra showed typical amide I and amide II absorption within the cell, while such bands were not observed outside of the cell (Fig. 4C and Fig. S8). The latter underscores that whole-cell spectroscopy reports exclusively on [FeFe]-hydrogenase located inside the cells, in agreement with biochemical assays previously reported.<sup>36</sup>

In the next step, we used attenuated total reflection Fourier-transform infrared (ATR FTIR) spectroscopy to probe the catalytic competence of cells in hydrated films. Cells containing [2Fe]<sup>adt</sup>-HydA1 were deposited on the silicon crystal of the ATR optic, dried under  $\text{N}_2$ , and rehydrated to form a film that can interact with gases. When the film was kept under  $\sim 100$  mbar deuterium gas ( $\text{D}_2$ ) instead of pure  $\text{N}_2$ , deuterium ions ( $\text{D}^+$ ) were released into bulk  $\text{H}_2\text{O}$ . The clear appearance of the HDO band ( $2515\text{ cm}^{-1}$ ) in ATR FTIR difference spectra served as direct verification of  $\text{D}_2$  oxidation activity (Fig. 4D),<sup>30</sup> confirming that the [FeFe]-hydrogenase located inside the cells retained its activity in hydrated films.

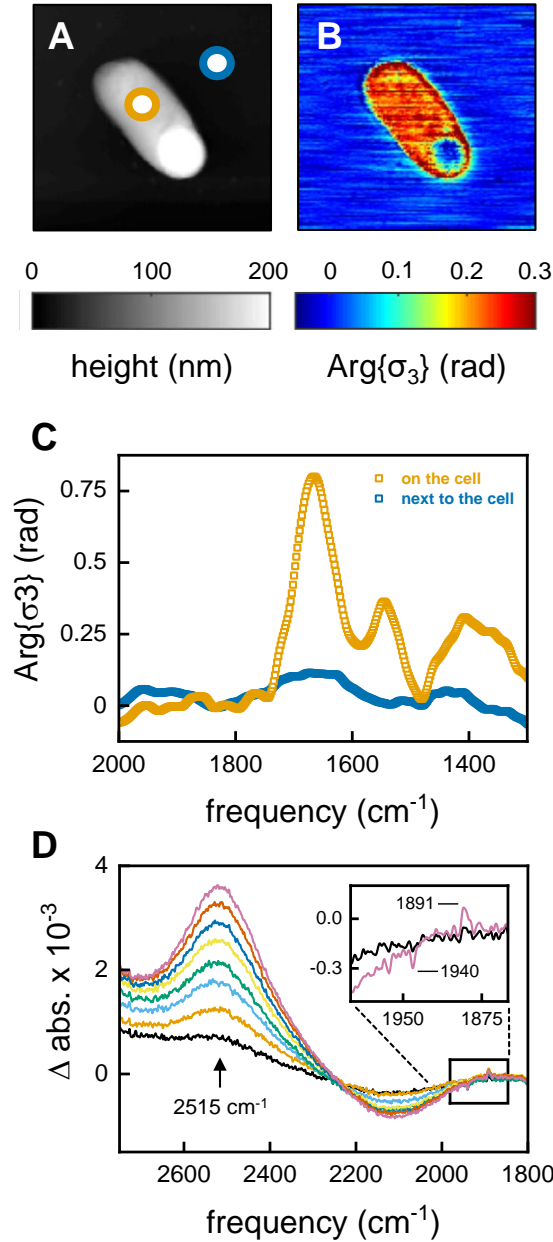


**Figure 4.** Single cell analysis. **(A)** AFM topography of a [2Fe]<sup>adt</sup> - HydA1 *E. coli* cell. **(B)** sSNOM image mapped at 1665 cm<sup>-1</sup> (amide I absorption). The protein is clearly localized to the cellular environment. The blue region in the cell most likely arises from debris on top of the cell. **(C)** Nano FTIR near field phase spectrum from 2000 – 1300 cm<sup>-1</sup>. Spectra were recorded on the cell and next to the cell (orange and blue circle in panel A). **(D)** ATR FTIR difference spectra showed an HDO band (2515 cm<sup>-1</sup>) increase in the presence of D<sub>2</sub> (exposure time 0 s – 90 s increasing from black to purple). **Inset:** A simultaneous enrichment of H<sub>red</sub> (1891 cm<sup>-1</sup>) over H<sub>ox</sub> (1940 cm<sup>-1</sup>) was observed in the CO/CN<sup>-</sup> regime of the spectrum (for clarity, only initial and final spectra shown).

**Mechanistic investigations on cell films using in situ ATR FTIR spectroscopy.** The H-cluster-specific CO and CN<sup>-</sup> vibrations in the region from 2150 – 1750 cm<sup>-1</sup> were clearly discernible in ATR FTIR spectroscopy. Films of [2Fe]<sup>adt</sup>-HydA1 containing *E. coli* showed a mixture of H<sub>ox</sub> and H<sub>ox</sub>-CO, in agreement with EPR results (Fig. S9). No trace of the free [2Fe]<sup>adt</sup> cofactor was detected. Exposing the film to 1% H<sub>2</sub> resulted in an enrichment of H<sub>red</sub> over H<sub>ox</sub> and H<sub>ox</sub>-CO on a time-scale of seconds, and increasing H<sub>2</sub> content to 100% had no further effects on the final spectra (Fig. 5A, spectrum a and Fig. S9). When H<sub>2</sub> was removed from the atmosphere (N<sub>2</sub> purging), the H-cluster converted back into H<sub>ox</sub> (Fig. 5A, spectrum b). The fact that H<sub>ox</sub>-CO does not re-appear suggests a high degree of cofactor stability on the time-scale of the FTIR measurements. Notably, neither H<sub>red</sub>' (CO marker band 1933 cm<sup>-1</sup>) nor H<sub>sred</sub> (CO marker band 1882 cm<sup>-1</sup>) were detected *in vivo*, in contrast to H<sub>2</sub> exposed films of purified [2Fe]<sup>adt</sup>-HydA1 (Fig. S10). When exposed to 1% CO, the oxidized whole-cell film converted to H<sub>ox</sub>-CO (Fig. 5A, spectrum c). The formation of H<sub>red</sub> and H<sub>ox</sub>-CO upon H<sub>2</sub> and CO flushing, respectively, is in agreement with the aforementioned EPR results on cell suspensions (Fig. 3).

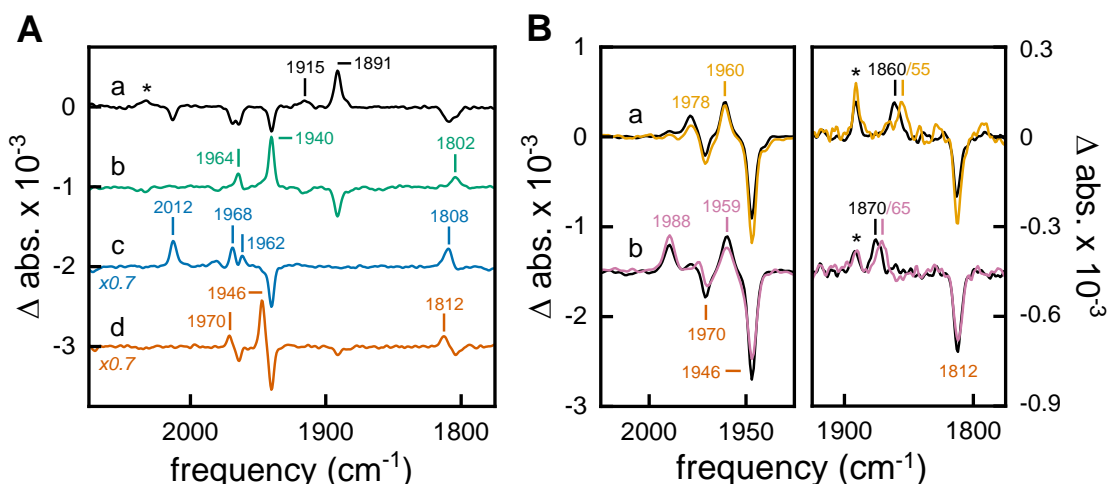


**Figure 5.** ATR FTIR analysis of  $[2\text{Fe}]^{\text{adt}}\text{-HydA1}$  containing cells. All difference spectra show the CO/CN<sup>-</sup> regime of the H-cluster. **(A)** In the presence of 1% H<sub>2</sub> (pH 8, 2 mM NaDT) freshly prepared cells converted from H<sub>ox</sub> and H<sub>ox</sub>-CO to H<sub>red</sub> (spectrum a). \* The band at 2032 cm<sup>-1</sup> was attributed to a CN<sup>-</sup> band of H<sub>red</sub>. In the absence of H<sub>2</sub> quantitative enrichment of H<sub>ox</sub> was observed (spectrum b). Exposure to 1% CO resulted in population of H<sub>ox</sub>-CO (spectrum c). Under non-reducing, acidic conditions (N<sub>2</sub>, pH 4, 2 mM NaDT) H<sub>ox</sub> converted into H<sub>ox</sub>H (spectrum d). **(B)** In the presence of 1% H<sub>2</sub> (pH 4, 2 mM NaDT) formation of H<sub>hyd</sub> over H<sub>ox</sub>H was observed (spectrum a, black line). Reduction with D<sub>2</sub> gas reproduced the hydride-specific downshift of the  $\mu\text{CO}$  band from 1860 to 1855 cm<sup>-1</sup> (spectrum a, dark yellow line). Increasing the NaDT in the aerosol to 100 mM (pH 4, 1% H<sub>2</sub>) facilitated accumulation of a novel species, H<sub>hyd</sub>H<sup>+</sup> (spectrum b, black line). The downshift of the  $\mu\text{CO}$  band under D<sub>2</sub> (1870 to 1865 cm<sup>-1</sup>) verified the presence of a hydride ligand (spectrum b, purple line). \* Cells adopt a small fraction of H<sub>red</sub> at low pH.

Acidification towards pH 4 in the presence of 2 mM sodium dithionite (NaDT) resulted in a total conversion of H<sub>ox</sub> into H<sub>ox</sub>H (Fig. 5A, spectrum d and Fig. S9).<sup>23</sup> In the presence of 1% H<sub>2</sub> or D<sub>2</sub>, a quantitative enrichment of H<sub>hyd</sub> over H<sub>ox</sub>H was observed (Fig. 5B, both spectra a). Increasing the NaDT concentration in the medium enabled detection of H<sub>hyd</sub> also at pH 8 (Fig. S11), suggesting that strongly reducing conditions allow the accumulation of this reactive intermediate also at weakly alkaline pH. Similar trends have been observed for the *in vitro* enrichment of H<sub>ox</sub>H and

$H_{red}H$ .<sup>23, 26</sup> The combination of high NaDT concentrations and acidic pH resulted in the formation of a new species, shifted to higher frequencies by up to  $15\text{ cm}^{-1}$  as compared to the previously reported  $H_{hyd}$  species (Fig. 5b, both spectra b). Low pH reference experiments on purified HydA1 in the presence of 100 mM NaDT and 1%  $H_2$  confirmed the possibility of generating this species also *in vitro*, which facilitated complete assignment of the band positions (Fig. S11). To verify that this new signal reflected a hydride-binding form of the H-cluster, the same species was generated using  $D_2$ , which resulted in the typical downshift of the bridging carbonyl band<sup>40</sup> from 1870 to  $1865\text{ cm}^{-1}$  (Fig. 5b, purple spectrum b).

Making use of *in situ* ATR FTIR spectroscopy on whole cells, we were able to observe several H-cluster species previously identified on purified hydrogenase. It is worth noting that, in contrast to *in vitro* conditions,  $H_{sred}$  and  $H_{red}$  were never observed, neither in alkaline nor acidic media. Conversely,  $H_{hyd}$  as well as the up-shifted hydride species readily accumulated under acidic conditions and could be selectively enriched as a function of NaDT concentration. A similar up-shifted hydride species has been reported earlier<sup>30, 40</sup> but remains to be fully characterized. Comparing its FTIR spectrum to that of  $H_{hyd}$  the observed spectral up-shifts are in good agreement with a protonation of the H-cluster. However, the magnitude of the shift is larger than those previously attributed to protonation changes at the  $[4Fe-4S]_H$  cluster (Fig. S11).<sup>23, 26</sup> Instead, DFT calculations have attributed shifts of similar magnitude to protonation changes at the  $[2Fe]_H$  subsite.<sup>40</sup> Thus, we assign this species to a hydride-state featuring a nitrogen protonated azadithiolate ligand,  $H_{hyd}H^+$ .

**A hydride-like species is formed under physiological conditions.** The formation of  $H_{\text{hyd}}$  in  $[2\text{Fe}]^{\text{adt}}$ -HydA1 containing cells was corroborated by EPR spectroscopy. Cell suspensions in weakly acidic NaDT-containing media, rapidly frozen after incubation with  $\text{H}_2$  revealed a rhombic signal ( $g_{zyx} = 2.075, 1.935, 1.881$ ) in good agreement with the *in vitro* identified  $H_{\text{hyd}}$  state (Fig. 6, spectrum a and Fig. S12).<sup>31, 40</sup> The broad nature of the low field feature observed at  $g \approx 2.08 - 2.05$  complicated an exact assignment of the  $g_z$  position but the  $g_y$  and  $g_x$  positions were readily apparent in spectra recorded at both 10 and 20 K (Fig. S13). As in the case of the  $\text{H}_2$  producing cell suspensions described above, small contributions from  $H_{\text{ox}}$  were still clearly visible in the spectrum, potentially in combination with an additional minor rhombic signal (see Fig. S12-14 for details). The observed shift of the  $H_{\text{ox}}$   $g_z$  position from 2.100 to 2.101 at low pH is arguably attributable to formation of  $H_{\text{ox}}\text{H}$ . Exposing apo-HydA1 containing cells to  $\text{H}_2$  in the presence or absence of NaDT did not result in any spectral features similar to  $H_{\text{hyd}}$ , neither did BL21(DE3) *E. coli* cells lacking the *hyda1* gene. The transient nature of the  $H_{\text{hyd}}$  state in cell suspensions was verified by exchanging the  $\text{H}_2$  atmosphere with Ar for 30 minutes, which resulted in a loss of  $H_{\text{hyd}}$  and conversion back to  $H_{\text{ox}}$ . The presence of NaDT in the cell medium during  $\text{H}_2$  treatment was beneficial but not strictly required for the generation of the  $H_{\text{hyd}}$  state (Fig. 6, compare spectra a and c). Increasing the NaDT concentration in the cell suspension up to 100 mM, i.e. conditions expected to favor accumulation of the aforementioned  $H_{\text{hyd}}\text{H}^+$  state, resulted in a more intense  $H_{\text{hyd}}$  signal but no distinct new spectral features were observed. In contrast, no  $H_{\text{hyd}}$  signal was discernible upon addition of 10 mM NaDT to the cell medium in the absence of  $\text{H}_2$  (Fig. 6, spectrum d).

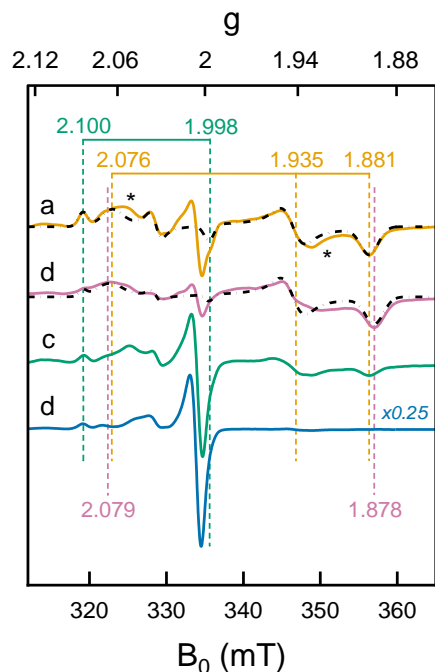


**Figure 6.** *In vivo* generation of the  $H_{\text{hyd}}$  and  $H_{\text{hyd}}^*$  states under different conditions probed by EPR spectroscopy. (a): The  $H_{\text{hyd}}$  state is observable in EPR spectra recorded on  $[2\text{Fe}]^{\text{adt}}\text{-HydA1}$  cells in pH 4 TRIS buffer complemented with 10 mM NaDT, flushed with  $\text{H}_2$  for 15 min and rapidly frozen (orange spectrum); (b): Samples prepared as lane a but at pH 7.5 gives rise to new signal attributed to the  $H_{\text{hyd}}^*$  state (purple spectrum); (c): Samples prepared as lane a but excluding NaDT generates a weaker  $H_{\text{hyd}}$  signal (yellow spectrum); (d): Samples prepared as lane a but excluding  $\text{H}_2$  flushing did not generate any discernable  $H_{\text{hyd}}$  species (blue spectrum). The g-values of  $H_{\text{ox}}$  (cyan dashed lines),  $H_{\text{hyd}}$  (orange dashed lines) and  $H_{\text{hyd}}^*$  (purple dashed lines) states are based on the simulations of the spectra (black dash-dotted lines), for details see Figure S12. Unassigned weak signals potentially attributed to an  $H_{\text{trans}}$ -like state indicated with asterisks.<sup>40</sup> EPR experimental conditions:  $T = 20$  K,  $P = 1$  mW,  $\nu = 9.38$  GHz.

A new rhombic,  $H_{\text{hyd}}$ -like, signal was observed when the analogous experiment was performed at pH 7.5 (Fig. 6, spectrum b and Fig. S12-S14). As it accumulates under conditions similar to those of  $H_{\text{hyd}}$ , we denote this species  $H_{\text{hyd}}^*$ . Similarly to the low pH  $H_{\text{hyd}}$ -signal, an exact assignment of the  $g_z$  position was challenging. Still, the spectrum featured a small but clearly discernible increased anisotropy, as compared to  $H_{\text{hyd}}$  ( $g_{zyx} = 2.079, 1.935, 1.878$ , vertical purple dashed lines in Fig. 6).

We have so far not been able to generate the equivalent state under *in vitro* conditions, and the structure of the species giving rise to this high pH signal remains to be elucidated. However, based on the similarity of the signal to that observed for the H<sub>hyd</sub>-state in particular,<sup>40</sup> but also the H<sub>trans</sub>-state,<sup>21</sup> it is attributed to a species featuring a reduced [4Fe-4S]<sub>H</sub> cluster coupled to a diamagnetic [Fe(II)Fe(II)]<sub>H</sub> subsite, closely resembling the H<sub>hyd</sub>-state. Finally, it is noteworthy that also H<sub>hyd</sub>\* was readily observable under an H<sub>2</sub> atmosphere even in the absence of NaDT, underscoring its physiological relevance.

## CONCLUSIONS

The artificial maturation of apo-HydA1 in *E. coli* provides access to high concentrations of [FeFe]-hydrogenase *in vivo*. Furthermore, cellular H<sub>2</sub> oxidation and production verify that the resulting semi-synthetic HydA1 enzyme is functional and connects to the cell metabolism, most likely *via* ferredoxins.<sup>6</sup> This has facilitated the first mechanistic investigation of an [FeFe]-hydrogenase under *in vivo* conditions, employing EPR and FTIR spectroscopy as complementary techniques. Despite differences in sample preparation and experimental conditions (i.e. cell suspension vs cell film, cryogenic vs ambient temperatures) both techniques reveal very similar trends.

The dominant oxidation states under alkaline conditions are H<sub>ox</sub> and H<sub>ox</sub>-CO in combination with a small fraction of an EPR-silent species. The latter was identified *via* FTIR spectroscopy as H<sub>red</sub> and could be enriched in the presence of H<sub>2</sub>. In experiments on hydrated cell films, this transition was rapid and quantitative but the enzyme converted back to H<sub>ox</sub> when H<sub>2</sub> was removed from the gas phase. Similar reactivity (“auto-oxidation”) is generally observed for HydA1 *in vitro*, and is clearly retained also *in vivo*. However, the whole-cell environment proved more divergent in the enzyme’s reactivity towards O<sub>2</sub>. It is well established that [FeFe]-hydrogenases are rapidly and

irreversibly damaged by O<sub>2</sub> under *in vitro* conditions.<sup>41-43</sup> Here, the cell suspension provides partial protection to the enzyme against aerobic degradation, similar to what has been observed when the enzyme is embedded in a protective redox gel.<sup>5</sup>

In addition to the relatively stable catalytic intermediates H<sub>ox</sub> and H<sub>red</sub>, the study revealed complex metal-hydride chemistry occurring *in vivo* and three different hydride species were observed. Acidification of the cell medium resulted in rapid formation of H<sub>ox</sub>H and exposing the acidified cells to reducing conditions resulted in accumulation of H<sub>hyd</sub>, previously observed *in vitro*. Moreover, the complementary nature of EPR and FTIR spectroscopy has allowed us to detect two additional hydride-like states, which we have denoted H<sub>hyd</sub>H<sup>+</sup> and H<sub>hyd</sub>\*. The existence of alternative hydride-like species has been suggested earlier from work on HydA1 amino acid variants with impaired proton transfer activity.<sup>30-31, 40</sup> Herein we show how a range of H<sub>hyd</sub>-like species can be selectively generated also in the fully functional enzyme, not only *in vitro* but also under intracellular conditions. EPR data clearly support the notion that an alternative hydride-like state, H<sub>hyd</sub>\*, is generated under physiological conditions, i.e. in the absence of dithionite and in weakly alkaline cell medium where the expected cytoplasmic pH is  $\approx 7.6$ .<sup>44</sup> The diverging pH dependence of H<sub>hyd</sub> and H<sub>hyd</sub>\* indicates that these species differ in protonation state somewhere in the vicinity of the H-cluster. However, we have not been able to sufficiently enrich this state for detection by FTIR spectroscopy and the site of protonation remains to be verified. In parallel, the assignment of H<sub>hyd</sub>H<sup>+</sup> as a hydride species is in good agreement with the observed H/D isotopic shift of the  $\mu$ -CO ligand. The pH dependence and spectral up-shift relative to H<sub>hyd</sub>, as well as earlier DFT calculations, strongly supports that this hydride features a protonated nitrogen bridgehead atom.<sup>40</sup> Additionally, a protonation on the [2Fe]<sub>H</sub> subsite rather than the [4Fe-4H]<sub>H</sub> cluster explains the absence of a distinct new signal in the corresponding EPR spectrum, as the latter reports

primarily on the paramagnetic  $[4\text{Fe-4S}]_{\text{H}}^+$  cluster. The possibility to accumulate this species also *in vitro* should enable more detailed studies, but  $\text{H}_{\text{hyd}}\text{H}^+$  potentially represent the first isolatable intermediate in the transition from  $\text{H}_{\text{ox}}$  to  $\text{H}_{\text{hyd}}$  following heterolytic  $\text{H}_2$  cleavage.

In conclusion, the expansion of artificial maturation to whole-cell conditions in combination with our capacity to manipulate and spectroscopically investigate  $[\text{FeFe}]$ -hydrogenases *in vivo* has allowed us to verify the physiological relevance of a number of proposed catalytic intermediates. Two new metal hydride species have been observed, under acidic and weakly alkaline conditions, respectively. Deciphering and understanding these intermediates represents an exciting future prospect, expected to provide critical insight into the reduced states of the catalytic cycle.

## EXPERIMENTAL SECTION

**General.** All chemicals were purchased from Sigma-Aldrich or VWR and used as received unless otherwise stated. All anaerobic work was performed in an MBRAUN glovebox ( $[\text{O}_2] < 10$  ppm). The expression vector encoding the *hydA1* gene (pETDuet-CrHydA1-His) was kindly provided by Prof. Marc Fontecave (College de France, Paris/CEA, Grenoble).  $(\text{Et}_4\text{N})_2[\text{Fe}_2(\text{adt})(\text{CO})_4(\text{CN})_2]$  ( $[\text{2Fe}]^{\text{adt}}$ ) was synthesized in accordance to literature protocols with minor modifications, and verified by FTIR spectroscopy.<sup>45-48</sup> The complex was dissolved in anaerobic potassium phosphate buffer (100 mM, pH 6.8) at 10 ng/ $\mu\text{L}$  - 10  $\mu\text{g}/\mu\text{L}$  concentration and used directly. Protein content was analyzed by 10% SDS- PAGE minigels in a BioRad Mini-PROTEAN Tetra Cell system. The proteins were stained with Page Blue protein staining solution (Thermo Fisher Scientific) according to the supplier's instructions.

**Overexpression of the apo-HydA1 hydrogenase.** *Escherichia coli* BL21(DE3) cells containing the HydA1 plasmid were grown in 50 mL M9 medium [22 mM Na<sub>2</sub>HPO<sub>4</sub>, 22 mM KH<sub>2</sub>PO<sub>4</sub>, 85 mM NaCl, 18 mM NH<sub>4</sub>Cl, 0.2 mM MgSO<sub>4</sub>, 0.1 mM CaCl<sub>2</sub>, 0.4% (v/v) glucose] under aerobic conditions until O.D.<sub>600</sub>=0.6 – 0.8 in the presence of ampicillin. The protein overproduction was induced with 1 mM IPTG and persisted at 20°C for 16-18 h with continuous aeration. The media was supplemented with 100 μM FeSO<sub>4</sub> at the time of the induction. Final O.D.<sub>600</sub> of the cultures were 1.4±0.2.

**In vivo formation of [2Fe]<sup>adt</sup> -HydA1.** The preparation of the semi-synthetic hydrogenase was performed following a literature protocol with minor modifications.<sup>36-37</sup> The apo-HydA1 protein was expressed in 50 mL *E. coli* cultures as described in the “*Overexpression of the apo-HydA1 hydrogenase*” section. After the 16 – 18 h expression period the cells were harvested, deaerated and transferred to the glove-box. The cells were re-suspended in fresh M9 medium (2 mL final volume), and formation of [2Fe]<sup>adt</sup> -HydA1 was achieved by treating the cell suspensions with 100 μg (156 nmol) [2Fe]<sup>adt</sup> complex (80 mM final conc.), unless otherwise stated, for 1 h at 37°C under strictly anaerobic conditions.

**Whole cell EPR and FTIR sample preparation.** The 2 mL concentrated cell suspensions generated via the “*In vivo formation of [2Fe]<sup>adt</sup>-HydA1*” protocol were centrifuged and the cell pellet washed with 1 mL TRIS-HCl buffer (100 mM TRIS, 150 mM NaCl pH 7.5) three times under anaerobic conditions. For EPR samples the cells were diluted to a final volume of 400 μL with TRIS-HCl buffer after the washing protocol and transferred into EPR tubes. The tubes were capped and directly frozen in liquid nitrogen. In case of FTIR samples four separate 2 mL sample preparations were combined, concentrated and diluted to 400 μL with TRIS-HCl buffer and frozen in liquid nitrogen under anaerobic conditions.

**Gas flushing experiments.** The 2 mL concentrated cell suspensions generated via the “*In vivo formation of [2Fe]<sup>adt</sup>-HydA1*” protocol were centrifuged and the cell pellet washed with 1 mL TRIS-HCl buffer (100 mM TRIS, 150 mM NaCl pH 7.5) two times and finally taken up in 1 mL TRIS-HCl buffer (100 mM TRIS, 150 mM NaCl pH 7.5) in closed glass vials. The suspensions were flushed in the glass vials with different gasses for 1 h. The air treated samples were incubated on atmospheric oxygen for 1 h. After flushing, the cells were concentrated to 400  $\mu$ L and transferred into EPR tubes. The tubes were capped and directly frozen in liquid nitrogen.’

**Generation of the H<sub>hyd</sub> EPR samples.** The apo-HydA1 containing cells were activated as described above. After activation the cells were washed with TRIS-HCl buffer (100mM Tris, 150mM NaCl) and re-suspended 400  $\mu$ L buffer under anaerobic conditions. The pH of the TRIS-HCl buffer was either pH 7.5 or pH 4 according to the experiment, and verified before and after each flushing experiment. When indicated, the TRIS-HCl buffer was complemented with 10 mM Na-dithionite. The H<sub>2</sub> treated samples were flushed with H<sub>2</sub> gas for 15 min under anaerobic conditions. After flushing the cells were quickly transferred into EPR tubes. The tubes were capped and flash frozen in liquid nitrogen. Plating the cells on ampicillin enriched LB-agar plates as well as SDS page gel analysis was used to ensure the viability and integrity of the cells also under low pH conditions (Figure S15).

**Hydrogenase activity measurements.** *In vivo* and *in vitro* activity measurements were performed according to published protocols.<sup>36</sup> Hydrogen production was determined by analyzing the head-space gas, using a gas chromatograph (GC; PerkinElmer LLC, MA, USA) equipped with a thermal conductivity detector (TCD) and a stainless-steel column packed with Molecular Sieve (60/80 mesh). A calibration curve was established by injecting known amounts of hydrogen. The

operational temperatures of the injection port, the oven and the detector were 100 °C, 80 °C and 100 °C, respectively. Argon was used as the carrier gas at a flow rate of 35 mL min<sup>-1</sup>.

**EPR measurements.** The EPR spectra shown are representative signals from at least two individual experiments. The individual experiments show some preparation dependent differences, but the amplitude of these background signals are negligible compared to the signal intensity of the [2Fe]<sup>adt</sup> activated HydA1. Measurements were performed on a Bruker ELEXYS E500 spectrometer using an ER049X SuperX microwave bridge in a Bruker SHQ0601 cavity (Figures 2 and 3 + S1, S3-S4) or a Bruker EMX micro equipped with an EMX Premium bridge and an ER4119 HS resonator (Figure 6 + S14-16), both equipped with an Oxford Instruments continuous flow cryostat and using an ITC 503 temperature controller (Oxford Instruments). Measurement temperatures ranged from 10 to 20 K, using liquid helium as coolant, with the following EPR settings unless otherwise stated: microwave power 1 mW, modulation amplitude 1 mT, modulation frequency 100 kHz. The spectrometer was controlled by the Xepr software package (Bruker).

**EPR spectra processing, simulations and Spin quantification.** The EPR spectra were processed using the softwares Matlab (Mathworks, Inc) and QSoas.<sup>49</sup> Matlab served for converting the EPR files to ascii format, while QSoas was used to display the spectra as a function of g values, for visual inspection and subtraction of background signals emerging from the cells. The processed signals were used for figures 2, 3, 6, S3-4 and S12. The simulations were performed using the easyspin toolbox (5.2.23) within Matlab.<sup>50</sup> Other details of the procedure can be found in ref<sup>37</sup>.

**Infrared measurements.** For whole-cell ATR FTIR spectroscopy, 1 mL *E. coli* suspension was deposited on the silicon crystal of an ATR cell in the beam path of a commercial FTIR spectrometer (Bruker). All experiments were performed at ambient temperature (~24 °C) and pressure (~1 atm), in the dark, and on hydrated films. The cell suspension was dried under 100% N<sub>2</sub> gas and re-

hydrated with buffer solution (100 mM Tris-HCl, MES, and PIPPS) in the humidified gas stream (aerosol), similar to what was reported for purified protein earlier.<sup>23</sup> The utilized buffer mix allowed titrating the cell film between pH 9 and pH 3. Reduction of [FeFe]-hydrogenase in the cells was induced by adding 1% - 100% H<sub>2</sub> to the N<sub>2</sub> gas stream (flow volume 1.5 L min<sup>-1</sup>). In the absence of H<sub>2</sub> (100% N<sub>2</sub>), the oxidized resting state (H<sub>ox</sub> or H<sub>ox</sub>H) recovered due to auto-oxidation. Transitions were followed with a spectral precision of 2 cm<sup>-1</sup> and 1,000 averages of interferometer scans per spectrum. Difference spectra were calculated by subtraction of single absorbance spectra recorded under varying conditions (e.g., H<sub>2</sub> – N<sub>2</sub>, pH 4 – pH 8, etc.).

For single-cell AFM, sSNOM and nano-FTIR cell suspensions were diluted by 1:20,000 and a 1 mL droplet was dried on template stripped gold substrate. Topographies, near-field maps and spectra were acquired under ambient conditions. For other technical details, the setup is described in the supplementary material section, Figure S16.

## **ASSOCIATED CONTENT**

### **Supporting Information**

The Supporting Information is available free of charge on the ACS Publications website. This includes additional EPR and FTIR data, AFM images of *E. coli* cells, in vitro enzymatic assay data, as well as an overview of the sSNOM and nanoFTIR setup.

## **AUTHOR INFORMATION**

### **Corresponding Author**

Dr. G. Berggren, Molecular Biomimetics, Dept. of Chemistry – Ångström Laboratory; Uppsala University; Lägerhyddsvägen 1, SE-75120, Uppsala, Sweden; E-mail: [gustav.berggren@kemi.uu.se](mailto:gustav.berggren@kemi.uu.se)

Dr. S. T. Stripp, Institute of Experimental Physics, Experimental Molecular Biophysics; Freie Universität Berlin; Arnimallee 14, DE-14195, Berlin, Germany; E-mail: [svен.stripp@fu-berlin.de](mailto:svен.stripp@fu-berlin.de)

### **Author Contributions**

‡These authors contributed equally.

### **Notes**

The authors declare no competing financial interests.

### **ACKNOWLEDGMENT**

The ERC (GB, StG contract no. 714102) and the Olle Engkvist Byggmästare foundation (GB and LM) are gratefully acknowledged for funding. The Deutsche Forschungsgemeinschaft is acknowledged for financial support to STS (STR 1554/5-1) and JH (HE 2063/5-1). Part of the project is funded by the Deutsche Forschungsgemeinschaft (DFG, German Research Foundation) under Germany's Excellence Strategy – EXC 2008/1 (UniSysCat) – 390540038 to JH.

### **REFERENCES**

1. Madden, C.; Vaughn, M. D.; Díez-Pérez, I.; Brown, K. A.; King, P. W.; Gust, D.; Moore, A. L.; Moore, T. A., Catalytic Turnover of [FeFe]-Hydrogenase Based on Single-Molecule Imaging. *J. Am. Chem. Soc.* **2012**, *134* (3), 1577-1582.
2. Lubitz, W.; Ogata, H.; Rüdiger, O.; Reijerse, E., Hydrogenases. *Chem. Rev.* **2014**, *114* (8), 4081-4148.
3. Hambourger, M.; Gervaldo, M.; Svedruzic, D.; King, P. W.; Gust, D.; Ghirardi, M.; Moore, A. L.; Moore, T. A., [FeFe]-Hydrogenase-Catalyzed H<sub>2</sub> Production in a Photoelectrochemical Biofuel Cell. *J. Am. Chem. Soc.* **2008**, *130* (6), 2015-2022.

4. Krishnan, S.; Armstrong, F. A., Order-of-magnitude enhancement of an enzymatic hydrogen-air fuel cell based on pyrenyl carbon nanostructures. *Chem. Sci.* **2012**, *3* (4), 1015-1023.
5. Plumeré, N.; Rüdiger, O.; Oughli, A. A.; Williams, R.; Vivekananthan, J.; Pöller, S.; Schuhmann, W.; Lubitz, W., A redox hydrogel protects hydrogenase from high-potential deactivation and oxygen damage. *Nat Chem* **2014**, *6* (9), 822-827.
6. Wegelius, A.; Khanna, N.; Esmieu, C.; Barone, G. D.; Pinto, F.; Tamagnini, P.; Berggren, G.; Lindblad, P., Generation of a functional, semisynthetic [FeFe]-hydrogenase in a photosynthetic microorganism. *En. Environ, Sci.* **2018**, *11* (11), 3163-3167.
7. Esmieu, C.; Raleiras, P.; Berggren, G., From protein engineering to artificial enzymes - biological and biomimetic approaches towards sustainable hydrogen production. *Sustainable Energy & Fuels* **2018**, *2* (4), 724-750.
8. Simmons, T. R.; Berggren, G.; Bacchi, M.; Fontecave, M.; Artero, V., Mimicking hydrogenases: From biomimetics to artificial enzymes. *Coord. Chem. Rev.* **2014**, *270-271* (0), 127-150.
9. Tard, C.; Pickett, C. J., Structural and Functional Analogues of the Active Sites of the [Fe]-, [NiFe]-, and [FeFe]-Hydrogenases *Chem. Rev.* **2009**, *109* (6), 2245-2274.
10. Haumann, M.; Stripp, S. T., The Molecular Proceedings of Biological Hydrogen Turnover. *Acc. Chem. Res* **2018**, *51* (8), 1755-1763.
11. Greene, B. L.; Schut, G. J.; Adams, M. W. W.; Dyer, R. B., Pre-Steady-State Kinetics of Catalytic Intermediates of an [FeFe]-Hydrogenase. *ACS Catalysis* **2017**, *7* (3), 2145-2150.

12. Peters, J. W.; Lanzilotta, W. N.; Lemon, B. J.; Seefeldt, L. C., X-ray Crystal Structure of the Fe-Only Hydrogenase (CpI) from *Clostridium pasteurianum* to 1.8 Angstrom Resolution. *Science* **1998**, *282* (5395), 1853-1858.
13. Berggren, G.; Adamska, A.; Lambertz, C.; Simmons, T. R.; Esselborn, J.; Atta, M.; Gambarelli, S.; Mouesca, J. M.; Reijerse, E.; Lubitz, W.; Happe, T.; Artero, V.; Fontecave, M., Biomimetic assembly and activation of [FeFe]-hydrogenases. *Nature* **2013**, *499* (7456), 66-69.
14. Silakov, A.; Wenk, B.; Reijerse, E.; Lubitz, W., 14N HYSCORE investigation of the H-cluster of [FeFe] hydrogenase: evidence for a nitrogen in the dithiol bridge. *Phys. Chem. Chem. Phys.* **2009**, *11* (31), 6592-6599.
15. Nicolet, Y.; Piras, C.; Legrand, P.; Hatchikian, C. E.; Fontecilla-Camps, J. C., *Desulfovibrio desulfuricans* iron hydrogenase: the structure shows unusual coordination to an active site Fe binuclear center. *Structure* **1999**, *7* (1), 13-23.
16. Posewitz, M. C.; King, P. W.; Smolinski, S. L.; Zhang, L.; Seibert, M.; Ghirardi, M. L., Discovery of Two Novel Radical S-Adenosylmethionine Proteins Required for the Assembly of an Active [Fe] Hydrogenase. *J. Biol. Chem.* **2004**, *279* (24), 25711-25720.
17. King, P. W.; Posewitz, M. C.; Ghirardi, M. L.; Seibert, M., Functional Studies of [FeFe] Hydrogenase Maturation in an *Escherichia coli* Biosynthetic System. *J. Bacteriol.* **2006**, *188* (6), 2163-2172.
18. Shepard, E. M.; Mus, F.; Betz, J. N.; Byer, A. S.; Duffus, B. R.; Peters, J. W.; Broderick, J. B., [FeFe]-Hydrogenase Maturation. *Biochemistry* **2014**, *53* (25), 4090-4104.
19. Caserta, G.; Pecqueur, L.; Adamska-Venkatesh, A.; Papini, C.; Roy, S.; Artero, V.; Atta, M.; Reijerse, E.; Lubitz, W.; Fontecave, M., Structural and functional characterization of the hydrogenase-maturation HydF protein. *Nat Chem Biol* **2017**, *13* (7), 779-784.

20. Rao, G.; Tao, L.; Suess, D. L. M.; Britt, R. D., A [4Fe-4S]-Fe(CO)(CN)-l-cysteine intermediate is the first organometallic precursor in [FeFe] hydrogenase H-cluster bioassembly. *Nat. Chem.* **2018**, *10* (5), 555-560.
21. Albracht, S. P. J.; Roseboom, W.; Hatchikian, E. C., The active site of the [FeFe]-hydrogenase from *Desulfovibrio desulfuricans*. I. Light sensitivity and magnetic hyperfine interactions as observed by electron paramagnetic resonance. *J. Biol. Inorg. Chem.* **2006**, *11* (1), 88-101.
22. Silakov, A.; Reijerse, E. J.; Albracht, S. P. J.; Hatchikian, E. C.; Lubitz, W., The Electronic Structure of the H-Cluster in the [FeFe]-Hydrogenase from *Desulfovibrio desulfuricans*: A Q-band <sup>57</sup>Fe-ENDOR and HYSCORE Study. *J. Am. Chem. Soc.* **2007**, *129* (37), 11447-11458.
23. Senger, M.; Mebs, S.; Duan, J.; Shulenina, O.; Laun, K.; Kertess, L.; Wittkamp, F.; Apfel, U.-P.; Happe, T.; Winkler, M.; Haumann, M.; Stripp, S. T., Protonation/reduction dynamics at the [4Fe-4S] cluster of the hydrogen-forming cofactor in [FeFe]-hydrogenases. *Phys. Chem. Chem. Phys.* **2018**.
24. Bennett, B.; Lemon, B. J.; Peters, J. W., Reversible Carbon Monoxide Binding and Inhibition at the Active Site of the Fe-Only Hydrogenase. *Biochemistry* **2000**, *39* (25), 7455-7460.
25. Katz, S.; Noth, J.; Horch, M.; Shafaat, H. S.; Happe, T.; Hildebrandt, P.; Zebger, I., Vibrational spectroscopy reveals the initial steps of biological hydrogen evolution. *Chem. Sci.* **2016**, *7* (11), 6746-6752.
26. Senger, M.; Laun, K.; Wittkamp, F.; Duan, J.; Haumann, M.; Happe, T.; Winkler, M.; Apfel, U.-P.; Stripp, S. T., Proton-Coupled Reduction of the Catalytic [4Fe-4S] Cluster in [FeFe]-Hydrogenases. *Angew. Chem. Int. Ed.* **2017**, *56* (52), 16503-16506.

27. Sommer, C.; Adamska-Venkatesh, A.; Pawlak, K.; Birrell, J. A.; Rüdiger, O.; Reijerse, E. J.; Lubitz, W., Proton Coupled Electronic Rearrangement within the H-Cluster as an Essential Step in the Catalytic Cycle of [FeFe] Hydrogenases. *J. Am. Chem. Soc.* **2017**, *139* (4), 1440-1443.
28. Adamska, A.; Silakov, A.; Lambertz, C.; Rüdiger, O.; Happe, T.; Reijerse, E.; Lubitz, W., Identification and Characterization of the “Super-Reduced” State of the H-Cluster in [FeFe] Hydrogenase: A New Building Block for the Catalytic Cycle? *Angew. Chem. Int. Ed.* **2012**, *51* (46), 11458-11462.
29. Ratzloff, M. W.; Artz, J. H.; Mulder, D. W.; Collins, R. T.; Furtak, T. E.; King, P. W., CO-Bridged H-Cluster Intermediates in the Catalytic Mechanism of [FeFe]-Hydrogenase CaI. *J. Am. Chem. Soc.* **2018**, *140* (24), 7623-7628.
30. Winkler, M.; Senger, M.; Duan, J.; Esselborn, J.; Wittkamp, F.; Hofmann, E.; Apfel, U.-P.; Stripp, S. T.; Happe, T., Accumulating the hydride state in the catalytic cycle of [FeFe]-hydrogenases. *Nat. Comm.* **2017**, *8*, 16115.
31. Mulder, D. W.; Guo, Y.; Ratzloff, M. W.; King, P. W., Identification of a Catalytic Iron-Hydride at the H-Cluster of [FeFe]-Hydrogenase. *J. Am. Chem. Soc.* **2017**, *139* (1), 83-86.
32. Rumpel, S.; Sommer, C.; Reijerse, E.; Farès, C.; Lubitz, W., Direct Detection of the Terminal Hydride Intermediate in [FeFe] Hydrogenase by NMR Spectroscopy. *J. Am. Chem. Soc.* **2018**, *140* (11), 3863-3866.
33. Esselborn, J.; Lambertz, C.; Adamska-Venkatesh, A.; Simmons, T.; Berggren, G.; Noth, J.; Siebel, J.; Hemschemeier, A.; Artero, V.; Reijerse, E.; Fontecave, M.; Lubitz, W.; Happe, T., Spontaneous activation of [FeFe]-hydrogenases by an inorganic [2Fe] active site mimic. *Nat Chem Biol* **2013**, *9* (10), 607-609.

34. Siebel, J. F.; Adamska-Venkatesh, A.; Weber, K.; Rumpel, S.; Reijerse, E.; Lubitz, W., Hybrid [FeFe]-Hydrogenases with Modified Active Sites Show Remarkable Residual Enzymatic Activity. *Biochemistry* **2015**, *54* (7), 1474-1483.
35. Birrell, J. A.; Rüdiger, O.; Reijerse, E. J.; Lubitz, W., Semisynthetic Hydrogenases Propel Biological Energy Research into a New Era. *Joule* **2017**, *1* (1), 61-76.
36. Khanna, N.; Esmieu, C.; Meszaros, L. S.; Lindblad, P.; Berggren, G., In vivo activation of an [FeFe] hydrogenase using synthetic cofactors. *En. Environ, Sci.* **2017**, *10* (7), 1563-1567.
37. Mészáros, L. S.; Németh, B.; Esmieu, C.; Ceccaldi, P.; Berggren, G., In Vivo EPR Characterization of Semi-Synthetic [FeFe] Hydrogenases. *Angew. Chem. Int. Ed.* **2018**, *57* (10), 2596-2599.
38. Stripp, S. T.; Happe, T., How algae produce hydrogen—news from the photosynthetic hydrogenase. *Dalton Trans.* **2009**, (45), 9960-9969.
39. Amenabar, I.; Poly, S.; Nuansing, W.; Hubrich, E. H.; Govyadinov, A. A.; Huth, F.; Krutokhvostov, R.; Zhang, L.; Knez, M.; Heberle, J.; Bittner, A. M.; Hillenbrand, R., Structural analysis and mapping of individual protein complexes by infrared nanospectroscopy. *Nat. Comm.* **2013**, *4*, 2890.
40. Mulder, D. W.; Ratzloff, M. W.; Bruschi, M.; Greco, C.; Koonce, E.; Peters, J. W.; King, P. W., Investigations on the Role of Proton-Coupled Electron Transfer in Hydrogen Activation by [FeFe]-Hydrogenase. *J. Am. Chem. Soc.* **2014**, *136* (43), 15394-15402.
41. Kubas, A.; Orain, C.; De Sancho, D.; Saujet, L.; Sensi, M.; Gauquelin, C.; Meynial-Salles, I.; Soucaille, P.; Bottin, H.; Baffert, C.; Fourmond, V.; Best, R. B.; Blumberger, J.; Léger, C., Mechanism of O<sub>2</sub> diffusion and reduction in FeFe hydrogenases. *Nat Chem* **2017**, *9* (1), 88-95.

42. Ceccaldi, P.; Schuchmann, K.; Muller, V.; Elliott, S. J., The hydrogen dependent CO<sub>2</sub> reductase: the first completely CO tolerant FeFe-hydrogenase. *En. Environ, Sci.* **2017**, *10* (2), 503-508.
43. Stripp, S. T.; Goldet, G.; Brandmayr, C.; Sanganas, O.; Vincent, K. A.; Haumann, M.; Armstrong, F. A.; Happe, T., How oxygen attacks [FeFe] hydrogenases from photosynthetic organisms. *Proc. Natl. Acad. Sci. U.S.A.* **2009**, *106* (41), 17331-17336.
44. Wilks, J. C.; Slonczewski, J. L., pH of the Cytoplasm and Periplasm of Escherichia coli: Rapid Measurement by Green Fluorescent Protein Fluorimetry. *J. Bacteriol.* **2007**, *189* (15), 5601-5607.
45. Le Cloirec, A.; C. Davies, S.; J. Evans, D.; L. Hughes, D.; J. Pickett, C.; P. Best, S.; Borg, S., A di-iron dithiolate possessing structural elements of the carbonyl/cyanide sub-site of the H-centre of Fe-only hydrogenase. *Chem. Commun.* **1999**, (22), 2285-2286.
46. Lyon, E. J.; Georgakaki, I. P.; Reibenspies, J. H.; Darensbourg, M. Y., Carbon Monoxide and Cyanide Ligands in a Classical Organometallic Complex Model for Fe-Only Hydrogenase. *Angew. Chem. Int. Ed.* **1999**, *38* (21), 3178-3180.
47. Schmidt, M.; Contakes, S. M.; Rauchfuss, T. B., First Generation Analogues of the Binuclear Site in the Fe-Only Hydrogenases: Fe<sub>2</sub>(μ-SR)<sub>2</sub>(CO)<sub>4</sub>(CN)<sub>2</sub>. *J. Am. Chem. Soc.* **1999**, *121* (41), 9736-9737.
48. Li, H.; Rauchfuss, T. B., Iron Carbonyl Sulfides, Formaldehyde, and Amines Condense To Give the Proposed Azadithiolate Cofactor of the Fe-Only Hydrogenases. *J. Am. Chem. Soc.* **2002**, *124* (5), 726-727.
49. Fourmond, V., QSoas: A Versatile Software for Data Analysis. *Anal. Chem.* **2016**, *88* (10), 5050-5052.

50. Stoll, S.; Schweiger, A., EasySpin, a comprehensive software package for spectral simulation and analysis in EPR. *J. Magn. Reson.* **2006**, *178* (1), 42-55.

